Fuel 312 (2022) 122868

Contents lists available at ScienceDirect

Fuel

journal homepage: www.elsevier.com/locate/fuel

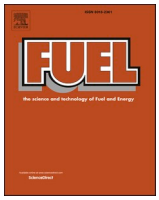

Full Length Article

Experimental investigation of naphthenic biofuel surrogate combustion in a compression ignition engine

Zhongnan Ran [a], Rodrigo Ristow Hadlich [a], Ruinan Yang [a], David C. Dayton [b], Ofei D. Mante [b], Dimitris Assanis [a,c,*]

[a] Department of Mechanical Engineering, Stony Brook University, Stony Brook, NY 11794, USA
[b] Technology Advancement & Commercialization, RTI International, Research Triangle Park, NC 27709, USA
[c] Advanced Energy Research and Technology Center, Stony Brook, NY 11794, USA

ARTICLE INFO

Keywords:
Naphthenic biofuel
Surrogate fuel
Bio-blendstock oil
Catalytic fast pyrolysis and hydrotreating pathway
Compression ignition combustion
Internal combustion engine

ABSTRACT

Biomass catalytic fast pyrolysis (CFP) integrated with hydrotreating (HT) produces advanced biofuels that could be used as bio-blendstocks to improve the properties of petroleum diesel fuels and enhance their combustion in compression ignition engines. The biofuels produced by CFP and HT are rich in naphthenes (cycloalkanes) that could improve cold-weather behavior and reduce the sooting propensity of blended diesel fuels. In this study, a surrogate fuel (SF1) that simulates a high-quality naphthenic bio-blendstock recovered from biomass CFP and HT was blended with research-grade No.2 diesel fuel (DF2) in different volume percentages and experimentally investigated in a single-cylinder Ricardo hydra diesel engine. Experiments were conducted by varying the fuel injection timings from the knock limit to the misfire limit at the same engine operating conditions for all of the SF1-DF2 blends (up to 40% by volume) and baseline No.2 diesel fuel. Engine output performance, combustion characteristics, and emissions including nitric oxides (NO_x), carbon monoxide (CO), total hydrocarbon (THC), and particulate matter (PM) were measured and analyzed. Experimental results showed that the surrogate blended at 10% and 20% by volume could yield comparable (<5%) engine output performance to that of baseline diesel at optimized fuel injection timings. Larger blend percentages (>20% & ≤40%) also exhibited good combustion controllability over a range of injection timings while sustaining a moderate reduction (~10–20%) in engine output performance compared to baseline diesel. Increasing surrogate fuel blend percentage resulted in higher CO, THC, and PM emissions as cetane number decreased and the combustion ignition delay increased. This correspondingly reduced and retarded the onset and magnitude of the heat release, increased the burn duration and reduced the peak cylinder pressures and temperatures during combustion also causing lower NO_x emissions for all SF1 blends. Results from the detailed experimental study ultimately indicate that based on the present surrogate fuel formulation representing a low-oxygenated naphthenic bio-blendstock produced from the CFP/HT pathway, such biofuels have the potential to be a viable drop-in fuel for compression ignition engines at moderate blend ratios without compromising engine performance and impacting exhaust emissions.

1. Introduction

The rapid increase of energy demand and consumption as a result of the increase in global population and industrial developments in recent decades has led to the accelerated depletion of non-renewable fossil fuel reserves and related adverse environmental impacts. In particular, the excessive utilization of fossil fuels for energy generation and transportation applications produces harmful emissions, like carbon dioxide (CO_2), nitrogen oxides (NO_x), hydrocarbon (HC), and particulate matters (PM), which lead to global warming and are detrimental to the health of human beings. Compression ignition (CI) engines are the primary propulsion system in transport, commerce, and power generation, mainly due to their superior thermal efficiency among the various types of internal combustion (IC) engines [1]. However, with increasing concerns over rising oil prices, accelerated depletion of fossil fuel reserves, and stringent emissions regulations from burning of diesel fuels

* Corresponding author.
E-mail address: dimitris.assanis@stonybrook.edu (D. Assanis).

https://doi.org/10.1016/j.fuel.2021.122868
Received 24 September 2021; Received in revised form 17 November 2021; Accepted 6 December 2021
Available online 21 December 2021

in CI engines, alternative low carbon fuels to conventional diesel fuel are in demand. The alternative fuel should be renewable, sustainable, environmentally friendly, and compatible with the current petroleum infrastructure. One of the most promising and economically achievable alternatives for the replacement of conventional fossil fuels is biofuels derived from biomass [2–5] because of their abundant supply, renewability, versatility, and CO_2 neutrality [6–8].

Biofuel derived from food crops, animal fats, or edible oils grown on arable lands using the transesterification technique is known as first-generation biodiesel [9]. However, the production of first-generation biodiesels suffers from restrictions and limitations, mainly due to controversial competition with the food industry and the need for large areas of arable land for plantation [6,10]. Therefore, in recent decades, there has been increased interest and focus on the development of biofuel technologies utilizing non-food-based biomass, such as forest resources, industrial and agricultural wastes, etc. [10].

Non-food biomass can be effectively converted into biofuels through direct thermochemical liquefaction processes such as gasification, pyrolysis, and hydrothermal liquefaction. Among the various types of technologies, pyrolysis is considered a promising method for converting solid biomass into liquid biofuel due to its simplicity and economic efficiency compared to other technologies [11]. However, due to the relatively high water content, oxygen content, acidity, and viscosity, the direct use of pyrolysis liquids derived from biomass as transportation fuels in IC engines present challenges [12,13].

Several experimental investigations have explored the potential of using biofuel derived from crude pyrolysis in CI engines. Shihadeh et al. experimentally studied the combustion characteristics of two pyrolysis bio-oils in a naturally aspirated Ricardo single-cylinder research engine. Their results show that the combustion of bio-oil achieved similar thermal efficiency with diesel, however, the ignition delay was much longer and combustion rates were slower [14]. Frigo et al. conducted experimental investigations of using modified pyrolysis oil in a single-cylinder Lombardini diesel engine. They found that combustion with crude pyrolysis oil resulted in coking of the fuel injector and thus inoperability of the direct injection system due to the formation of carbon deposits, as well as engine failure in extreme circumstances [15]. Due to the different physicochemical properties of crude pyrolysis-derived bio-oil compared to conventional liquid fossil fuels used in engines, the CI engine performance and combustion characteristics will be significantly affected if no modifications are made to the engine subsystems [16,17]. It can be concluded that the crude pyrolysis bio-oil from biomass needs to be upgraded to remove undesirable contents, such as water, oxygen, and other undesirable components.

Advanced direct thermochemical liquefaction processes such as catalytic fast pyrolysis (CFP), hydropyrolysis, and reactive catalytic fast pyrolysis (RCFP) have been shown to produce bio-oils with less oxygen content and high hydrocarbon content (aromatics) suitable for integrating into a conventional refinery without extensive pretreatment [10]. The bio-crudes produced from the catalyst-assisted processes like CFP have more favorable physicochemical properties than the non-catalytic derived pyrolysis bio-oil and they also contain fewer acids, oxygenates, and other undesirable compounds [18,19]. Nevertheless, the CFP biocrude still needs to be upgraded into finished drop-in transportation fuel for direct use in IC engines. The CFP bio-crude can be deoxygenated to produce finished fuel through hydrotreating [20]. Hydrotreating (HT) is an upgrading process that is effective at removing oxygen from biocrudes to produce hydrocarbon-rich refinery intermediates or infrastructure-compatible finished fuels [21–23]. The products of hydrotreating biocrude oils consist mainly of naphthenes, paraffins, aromatics, olefins, and some oxygenated compounds depending on the hydrotreating catalysts and process conditions. The upgraded product can be distilled to recover a bio-blendstock distillate boiling within the diesel range that is compatible with the current liquid hydrocarbon distribution and consumption infrastructure. Studies have shown that such bio-blendstock mid-distillate recovered from CFP and HT processes is rich in naphthenes, meets the ASTM D396 [24] specifications, and can be blended with No.2 diesel without affecting the combustion process [23]. Also, the bio-blendstock distillate has the potential to meet the ASTM D975 [25] specifications, and as such, it could be blended into base diesel fuel for IC engines.

However, there is a lack of detailed experimental studies investigating the use of the naphthenic bio-blendstock distillate produced through CFP and HT in IC engines. To bridge the gap, this work investigated the impact of blending a modeled naphthenic bio-blendstock with research-grade No.2 diesel (DF2) on combustion performance in a CI engine. A surrogate fuel (SF1) was developed from commercially available pure compounds based on the composition of a naphthenic bio-blendstock with an oxygen content of 1 wt%. SF1 was blended with DF2 at different volume percentages and experimentally investigated in a single-cylinder research diesel engine. The combustion, emissions, and cycle performance of these blends were evaluated and compared to conventional diesel performance under the same operating conditions. The insights and conclusions derived from this detailed experimental study of the bio-blendstock surrogate in a CI engine will help guide the development and production of future CFP/HT bio-blendstock oils that must meet the relevant ASTM specifications (e.g., D975 [25]) and the required in-cylinder performance needed for future transportation fuels.

2. Materials and methods

2.1. Production of bio-blendstock oil and surrogate fuel formulation

The surrogate fuel used for the engine testing was formulated based on the chemical composition of a bio-blendstock with 0.92 wt% oxygen content. The bio-blendstock was distilled from a liquid product obtained from the HT of a biocrude produced by CFP of loblolly pine. The CFP was performed over a gamma-alumina catalyst at 465 °C with an average biomass feed rate of 55 kg/h. The HT was performed over a sulfided NiMo based hydroprocessing catalyst in a 2-stage reactor configuration at 2000 psig and 0.25 h^{-1} liquid hourly space velocity at an average temperature of 300 °C. The design and operation of the 1 TPD (tons per day) catalytic biomass pyrolysis and the pilot-scale hydrotreating unit have been reported elsewhere [19,26,27] and details can be found in the literature. The distillation of the hydrotreated product was performed in a fully automated, processor-controlled bench-scale PILODIST laboratory distillation unit (PETRODIST 300 CC) with one theoretical stage column to recover the bio-blendstock boiling in mid-distillate range (160–360 °C).

The recovered bio-blendstock was then characterized by Gas Chromatography-Mass Spectrometry (GC–MS), Detailed Hydrocarbon Analysis (DHA) up to C15, Carbon Number Distribution, and Distillation using ASTM D86 [28] to determine the major chemical functional groups present to guide the surrogate formulation. The elemental composition (carbon [C], hydrogen [H], oxygen [O], nitrogen [N], and sulfur [S]) was also determined. A detailed description of the characterization methods is described in section 2.3. The oxygen content of the bio-blendstock was 0.92 wt.% per the CHNS analysis. Fig. 1 shows a summary chart of the GC–MS peak area percent for the chemical composition of the bio-blendstock. The results showed that it contained primarily naphthenic hydrocarbons, aromatic hydrocarbons (mono- di-, and poly-), and paraffins. The concentration of the phenols and other oxygenated aromatics was relatively low. Based on the carbon number distribution, the bio-blendstock contained C8-C20 hydrocarbons with 65 wt% concentrated within C8-C15. Furthermore, DHA (Table 1) showed that the hydrocarbon fractions up to C-15 contained about 26.5 wt% naphthenes, 3.4 wt% paraffins, 11.0 wt% aromatics, 0.6 wt% olefins, 6.7 wt% oxygenates, and about 0.5 wt% unknowns constituted the hydrocarbon fractions up to C-15. According to the ASTM D86 [28] distillation, about 95 vol% of the bio-blendstock boil below 350 °C.

The DHA result was used as a primary guide in the formulation of the surrogate fuel for engine testing. The GC–MS, carbon number

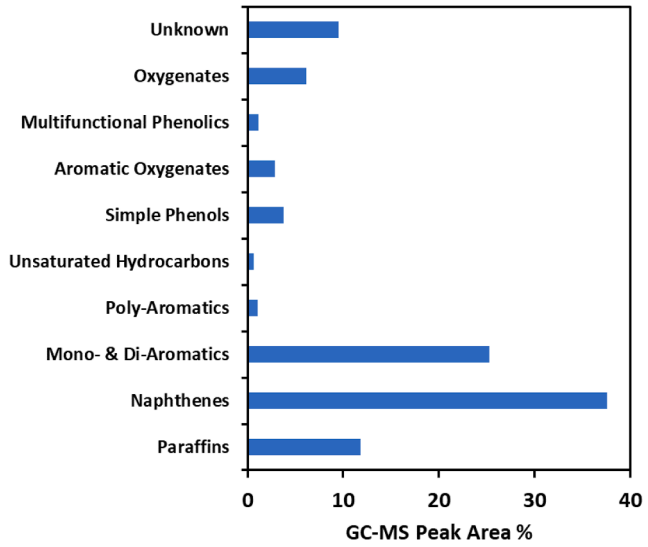

Fig. 1. GC–MS analysis of the recovered bio-blendstock with oxygen content of 0.92 wt%.

Table 1
DHA of bio-blendstock (Up to C15).

Compounds (<C15 Hydrocarbons)	wt.%
Paraffin	**2.67**
I-Paraffins	0.72
Aromatics	11.04
Mono-Aromatics	9.58
Naphthalenes	0.57
Indanes	0.90
Naphthenes	**26.46**
Mono-Naphthenes	18.81
Di/Bicyclo-Naphthenes	7.46
Olefins	0.60
n-Olefins	0.00
Iso-Olefins	0.06
Naphtheno-Olefins	0.54
Di-Olefins	0.01
Oxygenates	6.69
Unidentified	0.53
Total	48.71

distribution, and the distillation profile results were used to supplement and fill in the gaps in the DHA data. The formulation approach used focused on matching the distribution of 5 major functional chemical groups (paraffins, naphthenes, di-aromatics, polyaromatics, and phenolics) in the bioblendstock while targeting the oxygen content (1% by weight). Other approaches to formulating surrogate fuels include minimalist functional group (MFG) [29] and simplex-lattice mixture design [30]. The MFG approach focuses on matching functional hydrocarbon groups (CH_3, CH_2, CH, CH-CH_2, and C-CH). Of note, the approach of matching the hydrocarbon class distribution is widely used [31–33] and was therefore adopted in this study. The selection of each compound to represent the various functional groups was based on availability, cost, purity, and environmental, safety, and health considerations. Decane and octadecane were selected to represent paraffins while decalin was selected for naphthenes. Tetralin was for mono-aromatics and phenanthrene was for polyaromatic hydrocarbons. 4-methylphenol was selected to represent phenolics and oxygenates in general. Of note, propylcyclohexane was the predominant naphthene produced but due to its high cost, an alternative naphthene (decalin) in the bioblendstock was selected since it is cheaper and readily available. The distribution of the major compounds representing chemical classes of paraffins, naphthenes, di-aromatics, polyaromatics, and phenolics in the bio-blendstock as detailed in Table 2 was estimated based on the

Table 2
Chemical composition of the surrogate fuel SF1.

Chemical Compound	Functional Group	Formula	Wt. %
Decane	Paraffins	$C_{10}H_{26}$	4.5
Octadecane	Paraffins	$C_{18}H_{38}$	7.0
Decalin	Napthenes	$C_{10}H_{18}$	55
Tetralin	Di-aromatics	$C_{10}H_{12}$	25
Phenanthrene	Polyaromatics	$C_{14}H_{10}$	3.5
4-Methylphenol	Phenolics	C_7H_8O	5.0

chemical characterization results. Details on the purity and thermophysical properties of the commercial compounds are provided in the supplementary information. Organic elemental analysis and GC–MS analysis were performed to validate that the chemical makeup of prepared SF1 was similar to the bio-blendstock. The results, shown in Fig. 2, present GC–MS peak area as a percentage of the total classes of compounds identified. Note that multi-phenols and simple phenols are represented together under the phenolics compound class. Also, bulk properties such as density, cloud point, and smoke point of the surrogate fuel SF1 were compared to the bioblendstock as presented in Table 3. The density and the smoke point of the bioblendstock and SF1 were comparable within variance of −0.77% and 8.05%, respectively. The cloud point of SFI (-15.5 °C) did track that of the bioblendstock (-19.0 °C) very well with a reasonable error of 7.4%. In general, both fuels had comparable properties.

2.2. Research grade No.2 diesel and blends with SF1

A research-grade 2007 certification Ultra-Low Sulfur No.2 Diesel (DF2) sourced from Haltermann Solutions was used as the parent fuel for the engine testing. One large batch (~5L) of SF1 prepared was blended with DF2 at 10–40% by volume. In all, four 2.5L SF1/DF2 blends of DF2 containing 10%, 20%, 30%, and 40% of SF1 by volume were formulated using a splash blending technique and ensured that the contents were properly mixed using a pneumatic mixer. The organic elemental composition and selected physical properties including density, energy co content, and cloud point for the SF1, DF2, and the blends were determined.

Table 4 shows the measured thermophysical properties of DF2 and the prepared SF1 fuel. The results indicate that the cloud point performance of SF1 is slightly lower than DF2. In a cloud point test, a fuel with a lower value indicates better cold-weather performance than a fuel with a higher value. On the other hand, the results show that SF1 had a slightly lower smoke point than DF2. For the smoke point test, a higher value indicates less propensity to form soot, while for the YSI test a lower value is desired, and both the smoke point and the YSI measurements can be used to quantify the soot formation tendencies of fuel during the combustion process. Recent studies [34,35] have shown that PM

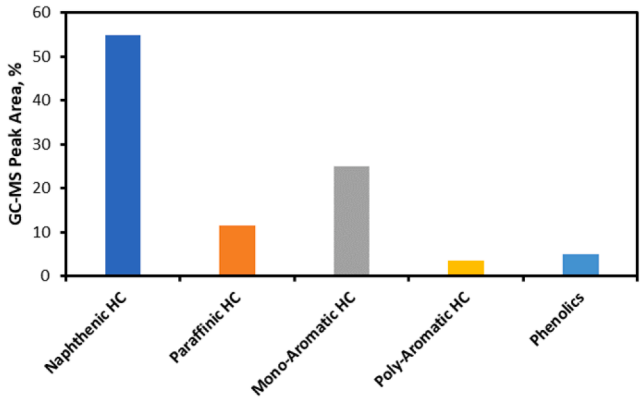

Fig. 2. GC–MS analysis of prepared surrogate fuel SF1.

Table 3
Measured properties of the bioblendstock and the formulated surrogate fuel SF1.

Fuel	Oxygen Content, wt%	Density (g/cm^3)	Cloud Point (° C)	Smoke Point (mm)
Bioblendstock	0.92	0.896	−19.00	14.90
SF1	1.00	0.902	−17.60	13.70
Variance/ Error	N/A	−0.77%	+7.40%	+8.05%

Table 4
Measured thermophysical properties of surrogate fuel SF1 and No.2 research diesel.

Thermophysical Property	Testing Method	SF1	DF2
Density @ 15 °C (kg/m^3)	ASTM D4052 [36]	902.1	851.3
Specific Gravity	ASTM D4052 [36]	0.9029	0.8521
Kinematic Viscosity (cSt)	ASTM D445 [37]	1.88	2.37
Cloud Point (℃)	ASTM D5773 [38]	−17.6	−16.3
Smoke Point (mm)	ASTM D1322 [39]	13.7	14.2
Yield Sooting Propensity (YSI/mass)	N/A	133	N/A
Higher Heating Value (MJ/kg)	ASTM D240 [40]	45.12	44.70
Ignition Delay Time (ms)	ASTM D8183 [41]	4.25	2.77
Indicated Cetane Number	ASTM D8183 [41]	32.6	46.6

emissions are directly related to the formation of soot in combustion flames, therefore, analysis and quantification of smoke point and YSI measurements for hydrocarbon type of fuels are crucial. Additionally, the prepared SF1 fuel shows a longer ignition delay time (IDT), as well as a significantly lower indicated cetane number (ICN) when compared with DF2. On the other hand, SF1 shows lower kinematic viscosity than baseline diesel fuel. The organic elemental composition of DF2, SF1, as well as the SF1/DF2 blends, including hydrogen to carbon (H/C) and estimated oxygen to carbon (O/C) ratio, are shown in Table 5. Furthermore, Table 6 compares the higher heating value (HHV), cloud point, density, kinematic viscosity, IDT, and ICN of all the fuels tested for the current experimental study. The addition of SF1 to DF2 up to 50 vol % changes the measured thermophysical properties of the blended fuels when compared with diesel. An increase in the volume of SF1 in the fuel blends resulted in an increase in density and a decrease in both HHV and cloud point. Additionally, increasing the SF1 content in fuel blends decreased both the kinematic viscosity and the indicated cetane number, while the ignition delay time was increased.

2.3. Characterization of Bio-blendstock oil & surrogate fuel

The organic elemental composition was determined with an elemental analyzer (FLASH2000, Thermo Scientific). The chromatography with mass spectrometric (GC–MS) analysis was conducted using an Agilent 6890GC and 5975C MS system. The GC–MS was equipped with an HP-5MS column (30 m × 0.25 mm, 0.25 μm film thickness with 5% phenyl-methyl-polysiloxane as the stationary phase). The National Institute of Standards and Technology (NIST) mass spectral library [42] was used to identify the most abundant compounds. Detailed Hydrocarbon Analysis (DHA) by ASTM D6729 [43] and boiling range

Table 5
Organic Elemental Analysis of fuels for engine testing.

Sample	% Carbon	% Hydrogen	H/C ratio	O/C ratio (est.)
DF2	87.1	12.8	1.76	–
SF1	87.3	11.7	1.61	0.0086
10%-SF1/DF2	87.2	12.6	1.74	0.0009
20%-SF1/DF2	87.1	12.6	1.73	0.0017
30%-SF1/DF2	87.1	12.5	1.72	0.0026
40%-SF1/DF2	87.5	12.1	1.65	0.0034
Measurement Uncertainty	± 1.0%	± 1.0%	± 0.04	est.

Table 6
Properties of SF1/DF2 blends for engine testing.

Sample	HHV (MJ/kg)	Cloud Point (℃)	Density @ 15℃ (kg/m^3)	Viscosity (cSt)	IDT (ms)	ICN
DF2	45.12	−16.3	851.3	2.37	2.77	46.56
SF1	44.70	−17.6	902.1	1.88	4.25	32.60
10%-SF1/DF2	45.06	−17.3	856.7	2.28	2.86	45.31
20%-SF1/DF2	44.96	−18.5	861.8	2.27	3.00	43.43
30%-SF1/DF2	44.88	−19.0	866.1	2.16	3.14	41.79
40%-SF1/DF2	44.72	−20.1	872.0	2.04	3.22	40.93

distribution by ASTM D2887 [44] were performed at Separation Systems Inc. (Gulf Breeze, FL). The D2887 [44] simulated distillation was from 50 °F to 1000 °F, including the Diesel range. The DHA was for PIANO (Paraffins, Isoparaffins, Aromatics, Naphthenes, and Olefins) groups up to n-C15. Carbon number analysis was performed using an Agilent HP6890 GC equipped with a flame ionization detector. A known amount of the sample was dissolved in 1.5 mL carbon disulfide. An Agilent DB-1 column with a 0.15-μm film thickness and 15 m in length was used. Calibration standards from C7 to C60 were used to identify the retention times of the various hydrocarbon species of interest and to assign peak groups to carbon numbers. A carbon number group was defined as the retention time from the end of the linear alkane peak in the immediately preceding group to the end of the linear alkane peak in the present group. The diesel fuel, surrogate fuel, and selected blends were evaluated for chemical and physical properties at several laboratories (Southwest Research Institute-SWRI, National Renewable Energy Laboratory-NREL, and Yale University) to determine the thermophysical properties of SF1 and DF2. Specifically, the ASTM D5773 [38] Cloud Point test was used for measuring cold-weather performance, and the ASTM D1322 [39] Smoke Point and aromatic Yield Sooting Index (YSI) tests were performed to determine sooting propensity. The Cloud Point test performed by NREL was obtained using a digital approach, which can yield a more repeatable measurement than the optical approach used in ASTM D2500 [45] certification tests. Higher heating values of all fuels were determined following the ASTM D240 [40] method. Additionally. The ASTM D4052 [36] test was used for the measurement of the density and specific gravity of all fuels at NREL, while the kinematic viscosity was measured at SWRI following the ASTM D445 [37] standard test. Organic elemental analysis was performed on the parent fuels DF2 and SF1, as well as the SF1/DF2 blend to determine the carbon, hydrogen, and oxygen content. Furthermore, the indicated cetane number, as well as the ignition delay time of DF2, SF1, and SF1/DF2 blends were determined at NREL by utilizing a constant-volume combustion chamber (CVCC) named the advanced fuel ignition delay analyzer (AFIDA) followed by the ASTM D8183-18 test standard [41]. More specifically, the test method utilizes a CVCC with direct fuel injection at 1000 bar into high temperature compressed air (580 °C and 17.5 bar) with 1.5 ms of injection duration for measurement of the IDT, and the ICN is then determined directly from IDT using an instrument-specific reference fuel empirical calibration equation [46,47]. The following equation, equation (1) shows the calibration equation used for the ICN measurements.

$$ICN = 98.094 \times IDT^{-4.394} + 101.051 \times IDT^{-0.785} \quad (1)$$

2.4. Engine experimental setup and methodology

Engine experimental tests were conducted using a single-cylinder,

compression ignition combustion research engine to assess the combustion characteristics, efficiencies, and emissions of the surrogate fuel compared to conventional research-grade No.2 diesel fuel. A production light-duty 1.7L GM engine head with a single-cylinder Ricardo Hydra research engine block was used. The engine head has four cylinders, but three of them were deactivated. The camshaft of the engine was modified to accommodate research requirements. The engine parameters, as well as the valve timings, are shown in Table 7, and a schematic for the experimental engine setup is displayed in Fig. 3.

Although the engine setup has a production head, the intake, exhaust, fuel, coolant, and oil systems are all custom-built to meet the needs of a research engine. It is connected to a 30 hp DC dynamometer, which is used to motor the engine and record torque data. Also, coupled with the crankshaft is a Kistler encoder, with a resolution of 0.1°, which serves as a trigger for the high-speed data measurements of all subsystems. All the low-speed measurements are recorded every two (2) seconds. Both the low and high-speed data are read using a custom LABVIEW data acquisition system (DAQ). The same DAQ is also used for controlling the heaters and radiators in the subsystems, as well as the injectors in the fuel system. The intake system consists of an air filter and an MCR Alicat mass flow meter to control and measure the mass flow rate of the incoming fresh air. A five (5) kW heater is placed downstream of the flow meter to heat the intake air whenever necessary. A plenum is placed upstream of the intake runner to prevent fluctuation in the intake air, ensuring accurate measurement of the air mass flow rate. Thermocouples are located at various locations for monitoring temperatures, and the intake pressure is measured through a high-speed Kistler pressure transducer located in the intake manifold.

A Bosch solenoid-type production diesel–fuel direct injector with 6 nozzle holes was used for the experimental study. The direct fuel injection system uses a common rail for directly injected fuel and is pressurized by a production Bosch CP3 high-pressure fuel pump. The CP3 pump can pressurize the fuel up to 2000 bar, and the fuel flow rate was measured using a Micro Motion Coriolis mass flow meter. The fuel injection pressure was measured by a high-speed Kistler pressure transducer located in the high-pressure fueling line. Detailed information regarding the direct fuel injector is listed in Table 8.

The exhaust system starts from the engine exhaust manifold and ends with the exhaust ventilation system. The system has a plenum-like intake system, after which a manually controlled throttle valve is located to control the exhaust pressure based on the experimental requirements. A high-speed, water-cooled pressure transducer has been installed in the exhaust manifold to read and record the pressure waves in the exhaust manifold. An oxygen sensor is located before the plenum to measure the oxygen content in the exhaust. The oxygen sensor is connected to an ECM Lambda CAN module, which is preprogrammed to calculate the air–fuel ratio based on the fuel composition input by the user. To measure the emissions in the exhaust, a sample of the exhaust gas is drawn from the exhaust plenum via a heated filtering line and directed to the Horiba MEXA 7100 D-EGR emissions bench for the measurement of the exhaust emissions, including NO_x, THC, CO, etc. [48] In addition, a TSI NanoScan (SMPS Nanoparticle Sizer) 3910 also draws a portion of the exhaust gas to measure the soot emissions from the engine, and it can measure particles from ten (10) to 420 nm. Additionally, the current engine setup includes an external exhaust gas recirculation (EGR) system, heated or cooled EGR can be supplied to the engine through the intake plenum and controlled by an electronic valve. However, EGR was not utilized in the current experimental study.

Table 7
Single-cylinder Ricardo Hydra compression ignition research engine parameters.

Bore	79 mm
Stroke	86 mm
Connecting rod length	160 mm
Engine displacement	421.5 cc
Compression ratio	15.1
Optical shaft encoder's resolution	0.1 (CAD)
Intake Valve Opening (IVO)	−354° deg aTDC
Intake Valve Closing (IVC)	−146° deg aTDC
Exhaust Valve Opening (EVO)	122° deg aTDC
Exhaust Valve Closing (EVC)	366° deg aTDC

Experimental investigation on the effects of fuel injection timing on engine combustion characteristics, performance, and emissions were studied using the Ricardo Hydra diesel engine. A fuel injection strategy consisting of a single injection event has been used for this experimental study. The fuel injection timings were varied from knock limit to misfire limit, at the same injection pressure, intake pressure, and temperature, and fuel–air equivalence ratio range. The knock limit (high load limit) is defined as when the maximum pressure rise rate (MPRR) began to exceed 10 bar/CAD, while the misfire limit (low load limit) was defined as the load at which the coefficient of variance (COV) of $IMEP_g$ exceeds 5%. Note that the crank angle degree (CAD) corresponding to misfire and knock limit varies for each blend, as shown in Fig. 5. The fuel injection pressure was fixed at 550 bar, while the intake air pressure and temperature were set at ambient conditions. A global fuel–air equivalence ratio (ϕ) was maintained at $\phi = 0.25$ for all fuels evaluated. The engine speed was fixed at 1200 revolutions per minute (RPM) throughout the experimental engine testing. A custom-built MATLAB post-processing program was used for the analysis of the collected 300 consecutive cycles of experimental data. Five different fuels were used for this study, including baseline research-grade No.2 diesel (referred to as DF2-Baseline) and the SF1/DF2 blends containing 10%, 20%, 30%, and 40% of pure SF1 by volume (the remaining volume was pure DF2, for example, 10%-SF1/DF2 referred to 10% of SF1 and 90% of DF2).

2.5. Uncertainty quantification

Uncertainty quantification is an important part of reporting experimental data as it demonstrates the confidence level of the measured and reported values. Errors can arise from many different sources, such as sensor accuracy, sensor calibration, changing environmental conditions, and reading of measured values to name a few. In complex systems such as an internal combustion engine research facility, the individual measurement errors must be minimized as they will be propagated through the subsequent calculations and analysis. The total uncertainty for each sensor or instrument is s determined using the root mean square error methodology and considers the accuracy error, resolution error, and precision error, where applicable, and summarized in Table 9 below.

It is also important to quantify the uncertainties associated with the tests performed to characterize the properties of the fuels reported in this work. Such tests were performed following the standardized procedures as outlined by ASTM International to ensure the highest confidence in the measure values. The total uncertainty for each testing procedure was also determined using the root mean square error methodology and considered the reproducibility error and repeatability error as outlined in the respective ASTM testing standard. Repeatability is defined by ASTM as "the difference between successive results obtained by the same operator in the same laboratory with the same apparatus under constant operating conditions on identical test materials", while reproducibility is defined as the "difference between two single and independent results obtained by different operators working in different laboratories on nominally identical test materials". The confidence interval for the fuel property measurements are listed and shown in Table 10 below.

3. Results and discussion

3.1. Engine combustion studies

3.1.1. Cylinder pressure and heat release profiles

The main parameters in engine combustion analysis are the pressure

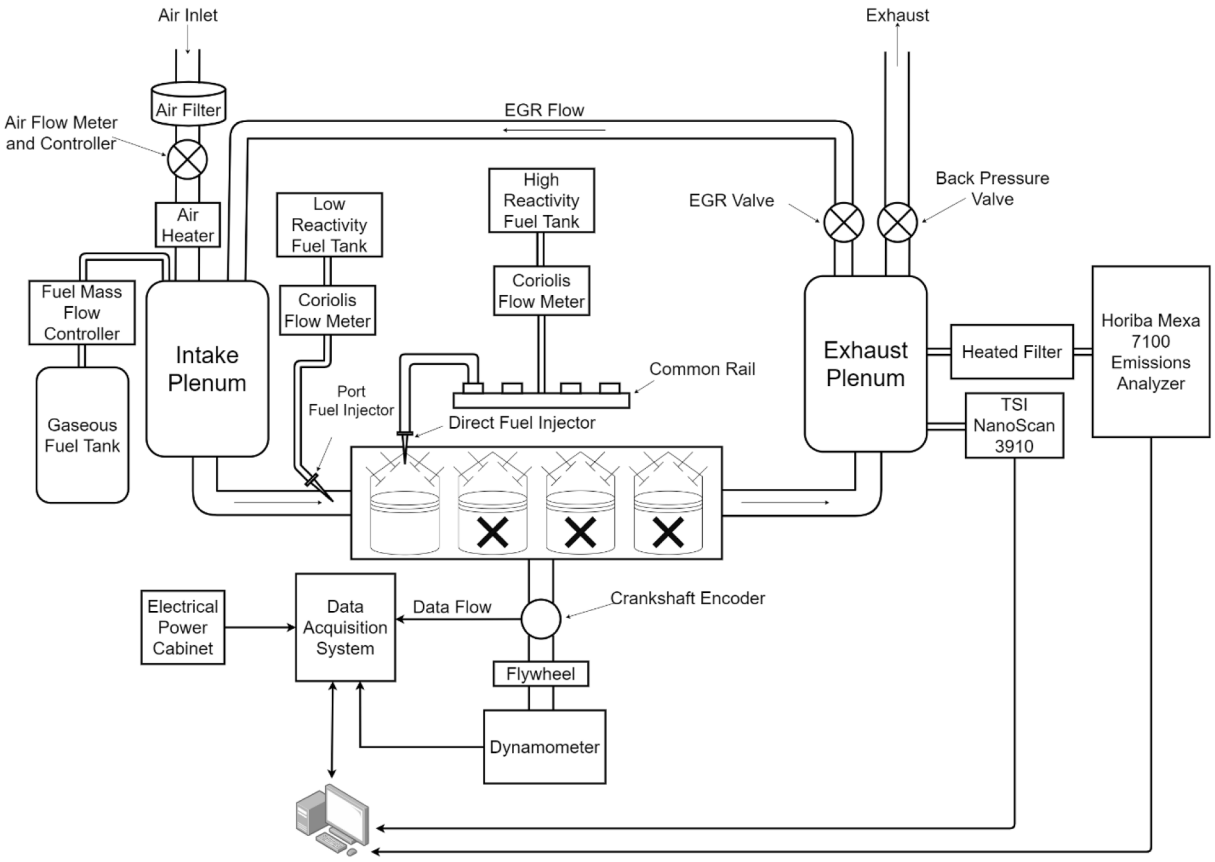

Fig. 3. Ricardo Hydra compression ignition combustion engine facility.

Table 8
Specifications for the direct fuel injector.

Number of nozzle holes	6
Nozzle diameter	130 μm
Spray included angle	150°
Spray type	Solid cone spray
Injection pressure	≤ 2000 bar
Injector mounting type	Centrally mounted

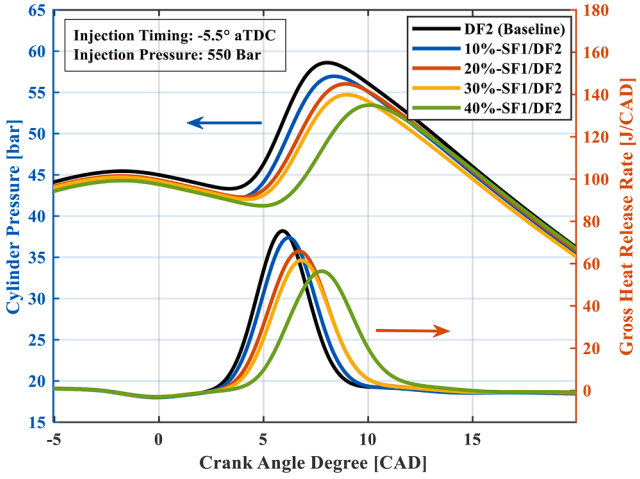

Fig. 4. Cylinder pressure and gross heat release rate as a function of crank angle degree.

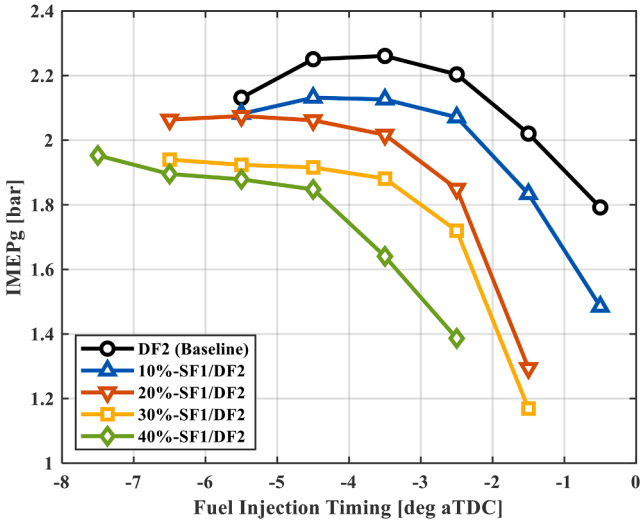

Fig. 5. $IMEP_g$ with varying injection timing for all fuel blends.

in the cylinder and the corresponding instantaneous volume of the cylinder. These two parameters are then used to calculate all other performance parameters, such as loads and efficiencies. The heat release rate is also very important as it indicates how much energy is being released from the fuel at each instant of the cycle. Fig. 4 presents the cylinder pressure and heat release rate as a function of CAD from −5 to 20°relative to the top dead center (TDC) for the same operating point (injection timing of 5.5°TDC) and all fuel blends. It can be seen in the figure that as the SF1 content is increased the heat release rate curve becomes more flattened (lower magnitude and longer duration) and that

Table 9
Measuring range and associated uncertainties for sensors and equipment.

Sensors/Instrument	Measuring Range	Uncertainty
Intake Pressure (Kistler 4011A)	0–5 bar	≤ ±0.5%
Cylinder Pressure (Kistler 6045B)	0–250 bar	≤ ±0.3%
Exhaust Pressure (Kistler 4049B)	0–5 bar	≤ ±0.5%
Signal Amplifier (Kistler 4665B)	N/A	≤ ±0.3%
Crankshaft Encoder (Kistler 2614C11)	0–12000 RPM	≤ ±0.00007
Dynamometer	0–4500 RPM	≤ ±0.1%
Lambda Sensor	0.04–2.5 (φ)	≤ ±0.9%
Micromotion Flow Meter	0–40.9 kg/h	≤ ±0.1% liquid
Alicat Mass Flow Controller MCRWH-1000SLPM-D/5M	0–1000 SLPM	≤ ±0.8% RD + ≤ ±0.2% FS
Thermocouples (Type K)	−200℃ to 1250℃	≤ ±0.75% RD
CO Emissions (Horiba MEXA 7100)	0–5000 ppm	≤ ±1.0%
NOx Emissions (Horiba MEXA 7100)	0–3000 ppm	
THC Emissions (Horiba MEXA 7100)	0–10000 ppm	
O2 Sensor (Horiba MEXA 7100)	0% − 18%	
CO2 Emissions (Horiba MEXA 7100)	0%-15%	

[a]Abbreviations stand for the percentage of full scale (% FS) and percentage of reading (% RD).

Table 10
Confidence interval for measured properties obtained during fuel analysis.

Fuel Properties Tested	Test Standard	Error/Bias
Kinematic Viscosity (cSt)	ASTM D445	≤ 2.31%
Higher Heating Value (MJ/kg)	ASTM D240	≤ 0.01%
DHA	ASTM D6729	≤ 0.07%
Boiling Range Distribution	ASTM D2887	≤ 0.03%
Cloud Point (℃)	ASTM D5773	≤ 0.17%
Smoke Point (mm)	ASTM D1322	≤ 0.25%
Density @ 15 °C (kg/m^3)	ASTM D4052	≤ 0.001%
Specific Gravity	ASTM D4052	≤ 0.001%
Ignition Delay Time (ms)	ASTM D8183	≤ 0.04%
Indicated Cetane Number	ASTM D8183	≤ 0.04%

the peak happens at a later position of the crankshaft, thus indicating a longer ignition delay. Due to the difference in the shape of the heat release profile, the pressure curve is also different for the blends. A larger content of SF1 yields a pressure curve with a lower peak and the peak happens at a more advanced crankshaft position. It can also be seen that the pressure decreases slightly faster for fuels with less SF1 in its formulation, and this is because the heat release happens in a smaller interval as opposed to a fuel with a high SF1 content, which will not reach as high peak pressure, but the pressure will decrease at a slower rate.

3.1.2. Engine load

There are many ways to measure engine load, but the most commonly used parameters are the Indicated Mean Effective Pressures (IMEP). The benefit of using IMEP is that it normalizes the output based on the size of the engine (i.e., the displaced volume), thus allowing for an evaluation of how efficient the engine is independent of its size. For this case, the Gross IMEP (IMEP$_g$) will be used since the goal of the experiment is to analyze the energy production part of the cycle (compression and expansion), hence the pumping part (intake and exhaust) is of no interest. Fig. 5 shows how the IMEP$_g$ changes with varying injection timing for all fuel blends. As can be seen in Fig. 5, starting from the knocking limit (left side), and moving towards misfire (right side), the peak IMEP$_g$ is in most cases in between both limits. In addition, the curves move to the left as the SF1 percentage increases, meaning that earlier injection timings are required to ensure stable combustion. The most important trend to notice here, however, is how IMEP$_g$ tends to drop with the increasing content of SF1. Since the IMEP$_g$ is directly related to the area under the curve of the Pressure-Volume diagram of the corresponding combustion cycle, this trend can be attributed to the longer ignition delay and burn duration experienced as the SF1 content increases, which causes a decrease in the heat release rate and thus lower cylinder pressures.

3.1.3. Gross thermal efficiency

The gross thermal efficiency is the ratio of the energy moving into the system in the form of chemical potential energy to the energy generated in the form of work. It is thus a measure of how successful the device is in transforming fuel into work, accounting for all forms of energy dissipation in the cylinder. Fig. 6 shows how the gross indicated thermal efficiency of each fuel changes with varying injection timing. The trend observed here is very similar to the one exhibited by IMEP$_g$ because these two parameters are coupled, so a higher thermal efficiency will lead to a higher load. The explanation for the drop in efficiency with increasing SF1 content can be given from the increase in ignition delay time and the decrease in the cetane number of SF1 compared to DF2, as shown in Table 6 and Fig. 7 in the following section. This increased ignition delay leads to a flatter rate of heat release curve and lower pressures, ultimately yielding a smaller work output from the cycle. And since the energy going into the system in the form of fuel–air mixture is the same in the combustion chamber, the thermal efficiency will then decrease.

3.1.4. Ignition delay

The ignition delay in compression ignition combustion is defined as the time it takes between the start of fuel injection (SOI) and the start of ignition of the fuel. The ignition delay is a very complex parameter that is affected by the cylinder conditions (pressure, temperature, swirl, injection pressure), as well as the fuel properties (molecular composition). Fig. 7 shows the behavior of the combustion ignition delay that was calculated based on measured cylinder pressure trace for all blends with varying injection timing. For all blends, the ignition delay increases when injection timing is delayed. This can be explained by the fact that the injection of fuel in this particular engine should take place very close to TDC (which is where peak compression temperature is found) for optimal load output without an excessive knock. This means that for the later injection timings presented, the cylinder temperature will peak when the fuel is injected but will quickly decrease after it reaches TDC. Ultimately, considering this particular operating range, injecting fuel later means the fuel will be exposed to high temperatures for less time,

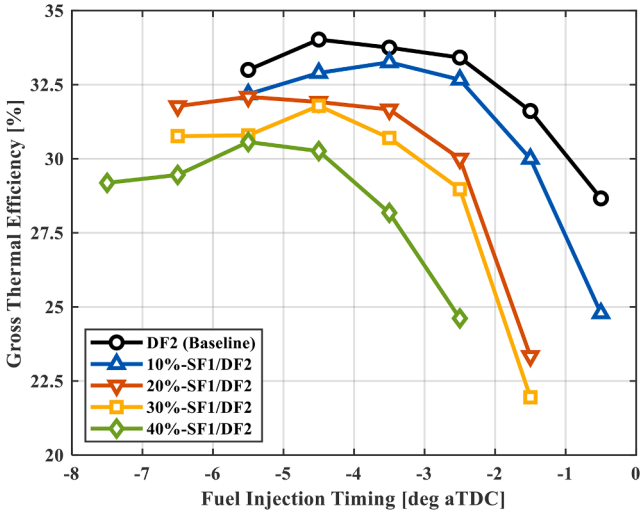

Fig. 6. Gross thermal efficiency with varying injection timing for all fuel blends.

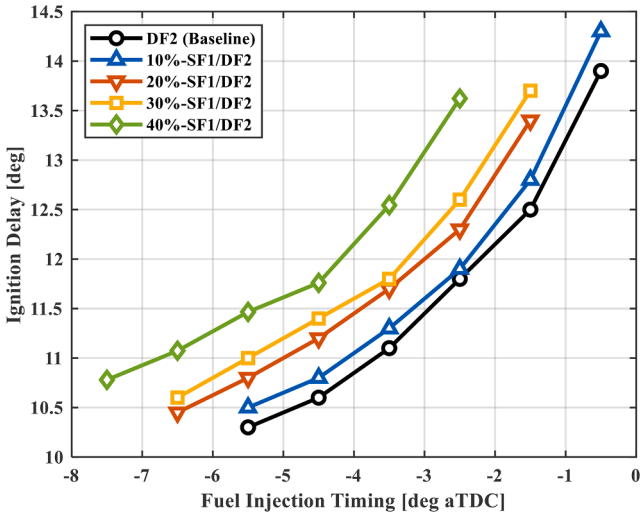

Fig. 7. Ignition delay with varying injection timing for all fuel blends.

and at a less favorable part of the ignition process, compared to the earlier injections. On the other hand, the ignition delay is also heavily affected by the chemical properties of the fuel itself, a behavior that is also present in the plot. Increasing the concentration of SF1 in the blend will also increase the combustion ignition delay, and this is mainly due to the increased ignition delay time and lower cetane number of the surrogate fuel as shown in Table 6 based on the measured values following the ASTM D8183[41] standard.

3.1.5. Combustion phasing and combustion duration (CA50 and CA10-90)

The crank angle position in which 50% of the mass of fuel in the cylinder has been burned (CA50) during the combustion process can be used as a parameter to indicate the combustion phasing. This parameter is strongly related to the ignition delay in diesel combustion, so it is anticipated that similar behavior will be observed as shown in Fig. 7. In addition, the crank angle interval between 10% and 90% (CA10-90) mass fraction burned is an indicator of the overall combustion duration. This parameter is also heavily affected by injection timing and fuel–air charge conditions due to the two distinct phases of fuel burn (pre-mixed and diffusion) that are found in conventional compression ignition combustion. Fig. 8 and Fig. 9 respectively present the experimental results obtained for the timing of occurrence of 50% mass fraction burned (CA50) and the overall duration (CA10-90) of combustion for all

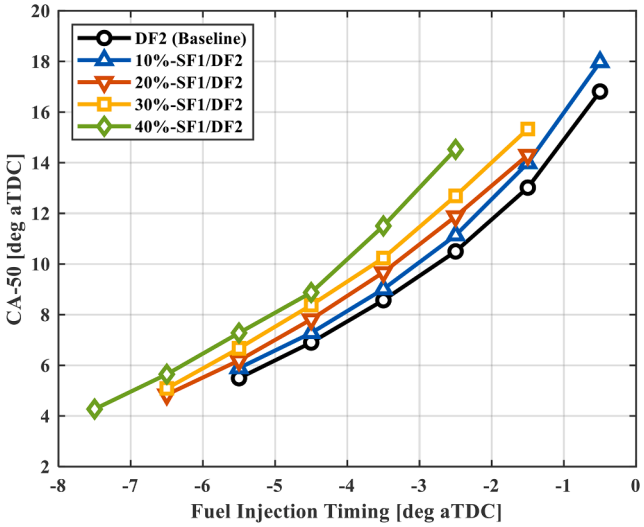

Fig. 8. CA50 with varying injection timing for all fuel blends.

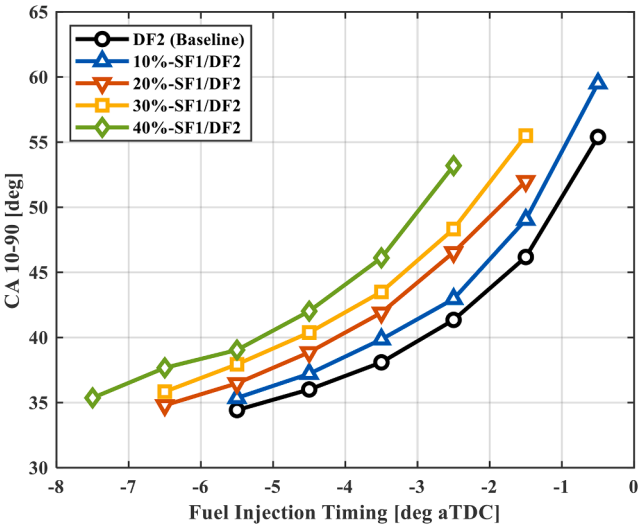

Fig. 9. CA10-90 with varying injection timing for all fuel blends.

surrogate fuel blends as a function of the injection timing.

The CA50 in Fig. 8 is shown to increase as injection timing is moved closer to TDC, and it does so in an exponential fashion. This is directly related to the ignition delay, seeing that the longer it takes for the fuel to start combusting, the longer it will take to reach the 50% fuel burned mark. Since increasing the SF1 content of the blend increases the ignition delay, it can also be seen that the CA50 happens at a later crank angle as the SF1 content increases.

The same behavior can be observed in Fig. 9. The CA10-90 becomes larger as injection timing is delayed because it is approaching misfire, which means the temperature and pressure in the cylinder are lower throughout the expansion stroke. This in turn causes the fuel to take longer to ignite when injected into the cylinder, thus leading to a longer burn duration. The plot also shows that an increased concentration of SF1 in the fuel blend yields a longer CA10-90. This is further supported by analyzing the heat release rate plot, shown on the bottom portion of Fig. 4, which shows that a blend with a higher SF1 content releases heat at a lower magnitude, along with a longer period of time, thus corresponding to the longer CA10-90.

3.1.6. Combustion efficiency

Combustion efficiency can be used to evaluate the consumption of the injected fuel mass during the in-cylinder combustion process. This efficiency can be measured by tracking the level of unburned THC and CO emissions present in the exhaust stream when combusting conventional hydrocarbon fuels. Additionally, this efficiency parameter is affected by the global air/fuel ratio, cylinder temperature, and pressure, as well as charge mixture thermophysical properties. Fig. 10 shows how combustion efficiency is affected by fuel injection timings for all fuel blends. It can be seen that combustion efficiency peaks at the earliest injection timings for all blends, thus this is the maximum attainable combustion efficiency for each case. It then decreases as the injection timing is retarded because the conditions inside the cylinder are not as favorable for combustion (lower temperatures and pressures). Also, the combustion efficiency drops as the SF1 content in the blend is increased, again due to the different physical and chemical characteristics introduced by the surrogate fuel. It was shown that increasing SF1 content leads to an increase in ignition delay, as well as longer combustion duration. These resulted in a heat release profile that reaches a lower peak but lasts for a longer period of time. The lower heat release rates mean that pressures and temperatures in the cylinder will be lower, hence fuel break-up and fuel–air mixing will be adversely affected, causing a reduction in combustion efficiency.

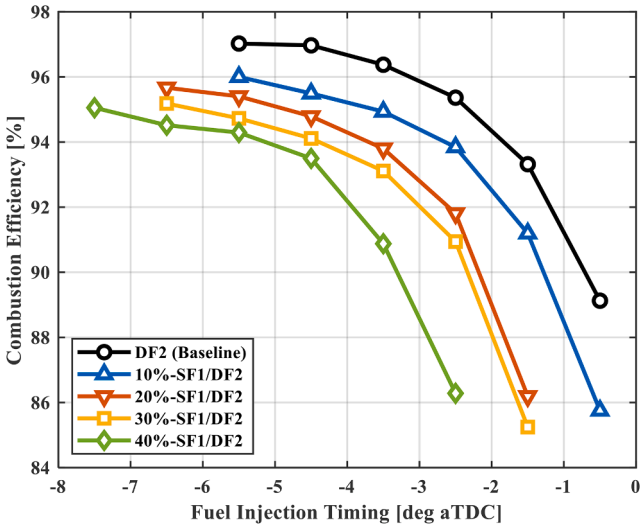

Fig. 10. Combustion efficiency with varying injection timing for all fuel blends.

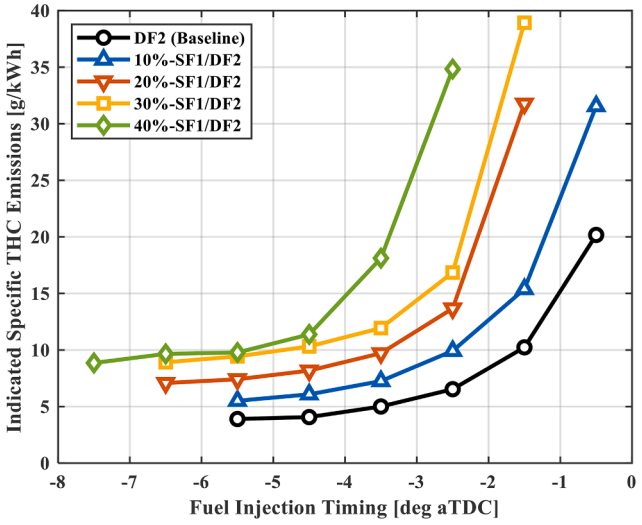

Fig. 12. Indicated specific THC emissions with varying injection timing for all fuel blends.

3.1.7. CO, THC, and NO_x emissions

It is also very important to consider the effect of the surrogate fuel on the emissions characteristics of the engine, compared with conventional diesel fuel. Fig. 11 and Fig. 12 respectively show the indicated specific emissions of CO and THC versus injection timing for all fuel blends and baseline diesel. As expected, the pattern observed is inversely proportional to that of the combustion efficiency, i.e., the emission of these gases increases as the injection timing is delayed towards TDC. This can be explained by the fact that CO and THC emissions are both incomplete combustion products, so the less efficient combustion is, the higher the concentration of these gases in the exhaust emissions. Another trend presented in Fig. 11 and Fig. 12 is that emissions concentrations of CO and THC increase as the blend ratio percentage increases due to the increasing concentration of SF1 present. This can be understood to be a consequence of the lower combustion efficiency achieved by increasing the concentration of the surrogate fuel, as a result of the overall lower cylinder pressures and temperatures caused by the longer ignition delay and the combustion duration.

Fig. 13 shows the indicated specific NO_x emissions as a function of fuel injection timing for all fuel blends evaluated. NO_x emissions are strongly correlated with the bulk in-cylinder peak combustion

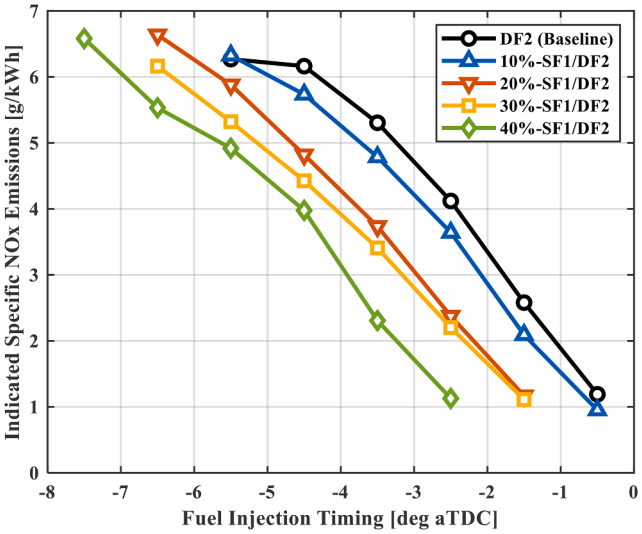

Fig. 13. NO_x emissions with varying injection timing for all fuel blends.

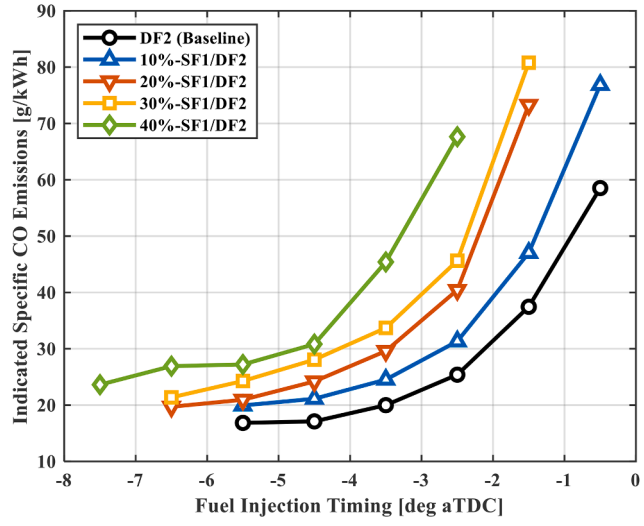

Fig. 11. Indicated specific CO emissions with varying injection timing for all fuel blends.

temperatures during combustion. Note the overall indicated specific NO_x emissions concentrations are extremely low, below 7 g/kWh, indicating that thermal formation of NO_x is at the minimum detection limit of the emissions analyzer. This is achievable because the peak in-cylinder combustion temperatures remain below the Zeldovich formation limit of 1800 K. Further, it can be observed in Fig. 13 that NO_x emissions decrease at a given blend percentage when the injection timing is retarded towards TDC. As the injection timing is delayed, the peak temperature reached in the cylinder is decreased due to a decrease in the peak cylinder pressure, which correspondingly results in lower cylinder bulk temperature and thus lower NO_x emissions. Lastly, as to blend ratio percentage increases, so does the concentration of SF1, which in turn produces a decreasing peak cylinder pressure and heat release rate as shown in Fig. 4. Thus, the peak cylinder temperatures decrease with increasing SF1 concentrations and hence the decrease in observed thermal NO_x formation.

3.1.8. PM emissions

In compression ignition engines, particulate matter (PM) emissions are a major concern, as these particles contribute to pollution of air,

formation of haze in cities and are detrimental to human health. Therefore, it is necessary to minimize the emission of these particles from CI engines during the combustion process, as well as in the exhaust emissions. Typical PM emissions from CI engines are divided into nucleation mode (PD < 50 nm) and accumulation mode (50 nm < PD < 1000 nm) based on their particle diameter (PD) size, and their formation is affected by many factors such as combustion process, fuel properties, and exhaust temperatures [49,50]. Currently, PM emissions produced from the combustion of conventional diesel fuel in modern CI engines can be effectively removed through diesel particulate filters (DPFs) to meet the stringent emissions regulations. However, as more soot accumulates in the DPF, the exhaust backpressure increases causing higher fuel consumption and increased engine stresses. DPFs ultimately have to regenerate by burning the excessive PM emissions trapped in the filter, a process that can be accomplished through engine calibration but comes at a cost reflected as a fuel-energy penalty. Therefore, it is important to find alternatives that can be used to replace conventional diesel fuel to eliminate the need for complex aftertreatments. Fig. 14 shows PM emissions as a function of fuel injection timings for diesel baseline and all SF1/DF2 fuel blends tested. The plot shows that the concentration of particles of diameters varies from 16 to 200 nm, with all measurements taken at a fixed fuel injection timing of 4.5°before TDC. It can be seen that baseline diesel fuel results in the lowest PM emissions of all fuels tested and increasing in the SF1 content resulted in higher PM concentration at the same diameter size. This behavior can be attributed to the overall lower smoke point, longer ignition delay time, as well as lower cetane number of the surrogate fuel, which results in a higher sooting propensity, longer fuel–air mixing time, and longer ignition delay during combustion. The latter leads to a slower heat release rate and a lower peak bulk cylinder temperature. Consequently, the surrogate fuel yields a lower combustion efficiency, which directly increases measured soot emissions.

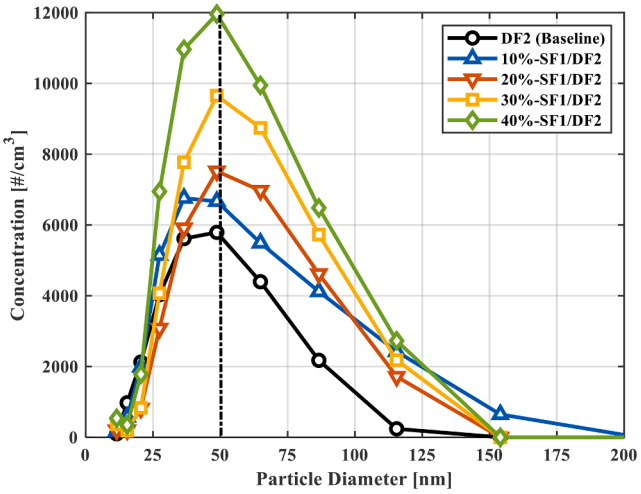

Fig. 14. Particle concentration of varying diameters at the constant injection timing.

4. Conclusions

In this study, experimental investigation of the effects of fuel injection timing on the combustion and emissions characteristics of a surrogate fuel (SF1) that simulates a high-quality naphthenic bio-blendstock recovered from biomass and blended with research-grade No.2 diesel fuel in different volumes percentages were conducted in a single-cylinder Ricardo hydra compression ignition combustion engine. During the experimental study, the fuel–air equivalence ratio was held constant at $\phi = 0.25$, the fuel injection pressure was fixed at 550 bar, with a constant engine speed of 1200 RPM, and the injection timing was chosen as the variable used to analyze and compare the combustion and emissions behavior of each blend. Experimental results obtained can be summarized as follows:

- A surrogate fuel that mimics a naphthenic bio-blendstock produced from woody biomass through the CFP/HT process can be used to replace part of the current petroleum-based diesel fuel in compression ignition combustion engines without major modifications to the infrastructure.
- The blending of the surrogate fuels with conventional No.2 diesel changes the measured thermophysical characteristics of the blended fuels. Measured properties show an increased ignition delay time, decreased cetane number, and decreased kinematic viscosity for increasing SF1/DF2 blend percentages.
- Due to the longer ignition delay time and lower cetane numbers of SF1 compared with diesel fuel. Overall fuel–air mixture combustion rate was reduced, resulting in lower and delayed heat release rates, thus increasing the burn duration, and lowering peak pressure and temperature for SF1/DF2 blends.
- Increasing the SF1 content in the fuel blends resulted in lower peak cylinder pressures and temperatures, which in turn decreased the gross indicated mean effective pressures and the gross thermal efficiencies compared with diesel fuel.
- Engine combustion efficiency is also affected by the lower peak bulk temperature in the cylinder, as a lower temperature results in slower fuel–air oxidation and combustion rate, and thus the combustion efficiency decreases when increasing the SF1 concentration.
- Higher SF1 content in the blended fuels resulted in lower peak combustion temperature, which leads to reduced NO_x emissions. However, decreased combustion efficiency leads to an increase in CO, THC, and PM emissions for increased SF1 blends.

CRediT authorship contribution statement

Zhongnan Ran: Investigation, Visualization, Writing – original draft. **Rodrigo Ristow Hadlich:** Investigation, Visualization, Writing – original draft. **Ruinan Yang:** Investigation. **David Dayton:** Investigation, Writing – review & editing. **Ofei Mante:** Conceptualization, Investigation, Visualization, Writing – review & editing. **Dimitris Assanis:** Supervision, Methodology, Data curation, Investigation, Writing – review & editing.

Declaration of Competing Interest

The authors declare that they have no known competing financial interests or personal relationships that could have appeared to influence the work reported in this paper.

Acknowledgements

All of the experimental studies were conducted at Stony Brook University as part of a CO-OPTIMA project funded by the United States Department of Energy, Energy Efficiency & Renewable Energy, award number DE-EE0008481. The authors would like to thank Gina Fioroni and Cameron Hays of the National Renewable Energy Laboratory for performing thermophysical property measurements and Dr. Charles McEnally and Prof. Lisa Pfefferle of Yale University for performing the Yield Sooting Index measurements.

Appendix A. Supplementary data

Supplementary data to this article can be found online at https://doi.org/10.1016/j.fuel.2021.122868.

References

[1] Reitz RD. Directions in internal combustion engine research. Combust Flame 2013; 160(1):1–8. https://doi.org/10.1016/j.combustflame.2012.11.002.

[2] Prakash R, Singh RK, Murugan S. Experimental studies on a diesel engine fueled with wood pyrolysis oil diesel emulsions. Int J Chem Eng Appl 2011;2:395–9. https://doi.org/10.7763/ijcea.2011.v2.141.

[3] Shrivastava P, Verma TN, Pugazhendhi A. An experimental evaluation of engine performance and emisssion characteristics of CI engine operated with Roselle and Karanja biodiesel. Fuel 2019;254:115652. https://doi.org/10.1016/j.fuel.2019.115652.

[4] Subramaniam M, Solomon JM, Nadanakumar V, Anaimuthu S, Sathyamurthy R. Experimental investigation on performance, combustion and emission characteristics of DI diesel engine using algae as a biodiesel. Energy Rep 2020;6: 1382–92. https://doi.org/10.1016/j.egyr.2020.05.022.

[5] Laesecke J, Ellis N, Kirchen P. Production, analysis and combustion characterization of biomass fast pyrolysis oil – Biodiesel blends for use in diesel engines. Fuel 2017;199:346–57. https://doi.org/10.1016/j.fuel.2017.01.093.

[6] Torri IDV, Paasikallio V, Faccini CS, Huff R, Caramão EB, Sacon V, et al. Bio-oil production of softwood and hardwood forest industry residues through fast and intermediate pyrolysis and its chromatographic characterization. Bioresour Technol 2016;200:680–90. https://doi.org/10.1016/j.biortech.2015.10.086.

[7] Amin A. Review of diesel production from renewable resources: Catalysis, process kinetics and technologies. Ain Shams Eng J 2019;10(4):821–39. https://doi.org/10.1016/j.asej.2019.08.001.

[8] Mohan D, Pittman CU, Steele PH. Pyrolysis of wood/biomass for bio-oil: a critical review. Energy Fuels 2006;20:848–89. https://doi.org/10.1021/ef0502397.

[9] Cho SM, Kim JH, Kim SH, Park SY, Kim JC, Choi IG. A comparative study on the fuel properties of biodiesel from woody essential oil depending on terpene composition. Fuel 2018;218:375–84. https://doi.org/10.1016/j.fuel.2018.01.021.

[10] Fermoso J, Pizarro P, Coronado JM, Serrano DP. Advanced biofuels production by upgrading of pyrolysis bio-oil. Wiley Interdiscip Rev Energy Environ 2017;6:1–18. https://doi.org/10.1002/wene.245.

[11] Si Z, Zhang X, Wang C, Ma L, Dong R. An overview on catalytic hydrodeoxygenation of pyrolysis oil and its model compounds. Catalysts 2017;7: 1–22. https://doi.org/10.3390/catal7060169.

[12] Lee S, Kim T, Kang K. Performance and emission characteristics of a diesel engine operated with wood pyrolysis oil. Proc Inst Mech Eng Part D J Automob Eng 2014; 228(2):180–9. https://doi.org/10.1177/0954407013502951.

[13] Mueller CJ. The feasibility of using raw liquids from fast pyrolysis of woody biomass as fuels for compression-ignition engines: a literature review. SAE Int J Fuels Lubr 2013;6(1):251–62. https://doi.org/10.4271/2013-01-1691.

[14] Shihadeh A, Hochgreb S. Diesel engine combustion of biomass pyrolysis oils. Energy Fuels 2000;14(2):260–74. https://doi.org/10.1021/ef990044x.

[15] Frigo S, Gentili R, Tognotti L, Zanforlin S, Benelli G. Feasibility of using wood flash-pyrolysis oil in diesel engines. SAE Tech Pap 1998. https://doi.org/10.4271/982529.

[16] Lehto J, Oasmaa A, Solantausta Y, Kytö M, Chiaramonti D. Review of fuel oil quality and combustion of fast pyrolysis bio-oils from lignocellulosic biomass. Appl Energy 2014;116:178–90. https://doi.org/10.1016/j.apenergy.2013.11.040.

[17] Lu Q, Li W-Z, Zhu X-F. Overview of fuel properties of biomass fast pyrolysis oils. Energy Convers Manag 2009;50(5):1376–83. https://doi.org/10.1016/j.enconman.2009.01.001.

[18] Iisa K, French RJ, Orton KA, Dutta A, Schaidle JA. Production of low-oxygen bio-oil via ex situ catalytic fast pyrolysis and hydrotreating. Fuel 2017;207:413–22. https://doi.org/10.1016/j.fuel.2017.06.098.

[19] Mante OD, Dayton DC, Gabrielsen J, Ammitzboll NL, Barbee D, Verdier S, et al. Integration of catalytic fast pyrolysis and hydroprocessing: a pathway to refinery intermediates and “drop-in” fuels from biomass. Green Chem 2016;18(22): 6123–35.

[20] Agblevor FA, Elliott DC, Santosa DM, Olarte MV, Burton SD, Swita M, et al. Red mud catalytic pyrolysis of pinyon juniper and single-stage hydrotreatment of oils. Energy Fuels 2016;30(10):7947–58. https://doi.org/10.1021/acs.energyfuels.6b0092510.1021/acs.energyfuels.6b00925.s002.

[21] Zacher AH, Olarte MV, Santosa DM, Elliott DC, Jones SB. A review and perspective of recent bio-oil hydrotreating research. Green Chem 2014;16(2):491–515.

[22] Wang H, Male J, Wang Y. Recent advances in hydrotreating of pyrolysis bio-oil and its oxygen-containing model compounds. Acs Catal 2013;3(5):1047–70.

[23] Mante OD, Butcher TA, Wei G, Trojanowski R, Sanchez V. Evaluation of biomass-derived distillate fuel as renewable heating oil. Energy Fuels 2015;29(10): 6536–43.

[24] ASTM D396-21, Standard Specification for Fuel Oils, ASTM International. West Conshohocken, PA,: 2021. doi: 10.1520/D0396-21.

[25] ASTM D975-21, Standard Specification for Diesel Fuel, ASTM International. West Conshohocken, PA,: 2021. doi: 10.1520/D0975-21.

[26] Dayton DC, Carpenter JR, Kataria A, Peters JE, Barbee D, Mante OD, et al. Design and operation of a pilot-scale catalytic biomass pyrolysis unit. Green Chem 2015; 17(9):4680–9.

[27] Mante OD, Dayton DC, Carpenter JR, Wang K, Peters JE. Pilot-scale catalytic fast pyrolysis of loblolly pine over γ-Al2O3 catalyst. Fuel 2018;214:569–79.

[28] ASTM D86-20b, Standard Test Method for Distillation of Petroleum Products and Liquid Fuels at Atmospheric Pressure. West Conshohocken, PA,: 2020. doi: 10.1520/D0086-20B.

[29] Jameel AGA, Naser N, Issayev G, Touitou J, Ghosh MK, Emwas A-H, et al. A minimalist functional group (MFG) approach for surrogate fuel formulation. Combust Flame 2018;192:250–71.

[30] Perez PL, Boehman AL. Experimental investigation of the autoignition behavior of surrogate gasoline fuels in a constant-volume combustion bomb apparatus and its relevance to HCCI combustion. Energy Fuels 2012;26(10):6106–17.

[31] Mueller CJ, Cannella WJ, Bruno TJ, Bunting B, Dettman HD, Franz JA, et al. Methodology for formulating diesel surrogate fuels with accurate compositional, ignition-quality, and volatility characteristics. Energy Fuels 2012;26(6):3284–303.

[32] Mueller CJ, Cannella WJ, Bays JT, Bruno TJ, DeFabio K, Dettman HD, et al. Diesel surrogate fuels for engine testing and chemical-kinetic modeling: Compositions and properties. Energy Fuels 2016;30(2):1445–61.

[33] Wu Z, Mao Y, Yu L, Wang S, Xia J, Qian Y, et al. Surrogate formulation for marine diesel considering some important fuel physical-chemical properties. Energy Fuels 2019;33(4):3539–50.

[34] Jiao Q, Anderson JE, Wallington TJ, Kurtz EM. Smoke point measurements of diesel-range hydrocarbon–oxygenate blends using a novel approach for fuel blend selection. Energy Fuels 2015;29(11):7641–9.

[35] Escudero F, Fuentes A, Demarco R, Consalvi J-L, Liu F, Elicer-Cortés JC, et al. Effects of oxygen index on soot production and temperature in an ethylene inverse diffusion flame. Exp Therm Fluid Sci 2016;73:101–8.

[36] ASTM D4052-18a, Standard Test Method for Density, Relative Density, and API Gravity of Liquids by Digital Density Meter, ASTM International,. West Conshohocken, PA,: 2018. doi: 10.1520/D4052-18A.

[37] ASTM D445-21, Standard Test Method for Kinematic Viscosity of Transparent and Opaque Liquids (and Calculation of Dynamic Viscosity), ASTM International,. West Conshohocken, PA,: 2021. doi: 10.1520/D0445-21.

[38] ASTM D5773-21, Standard Test Method for Cloud Point of Petroleum Products and Liquid Fuels (Constant Cooling Rate Method), ASTM International,. West Conshohocken, PA,: 2021. doi: 10.1520/D5773-21.

[39] ASTM D1322-19, Standard Test Method for Smoke Point of Kerosene and Aviation Turbine Fuel, ASTM International. West Conshohocken, PA,: 2019. doi: 10.1520/D1322-19.

[40] ASTM D240-19, Standard Test Method for Heat of Combustion of Liquid Hydrocarbon Fuels by Bomb Calorimeter, ASTM International,. West Conshohocken, PA,: 2019. doi: 10.1520/D0240-19.

[41] ASTM D8183-18, Standard Test Method for Determination of Indicated Cetane Number (ICN) of Diesel Fuel Oils using a Constant Volume Combustion Chamber—Reference Fuels Calibration Method, ASTM International. West Conshohocken, PA,: 2018. doi: 10.1520/D8183-18.

[42] Stein SE. National institute of standards and technology (NIST) mass spectral database and software 1990.

[43] ASTM D6729-20, Standard Test Method for Determination of Individual Components in Spark Ignition Engine Fuels by 100 Metre Capillary High Resolution Gas Chromatography, ASTM International. West Conshohocken, PA,: 2020. doi: 10.1520/D6729-20.

[44] ASTM D2887-19ae2, Standard Test Method for Boiling Range Distribution of Petroleum Fractions by Gas Chromatography,ASTM International. West Conshohocken, PA,: 2019. doi: 10.1520/D2887-19AE02.

[45] ASTM D2500-17a, Standard Test Method for Cloud Point of Petroleum Products and Liquid Fuels, ASTM International. West Conshohocken, PA,: 2017. doi: 10.1520/D2500-17A.

[46] Fioroni G, Fouts L, Luecke J, Vardon D, Huq N, Christensen E, et al. Screening of Potential Biomass-Derived Streams as Fuel Blendstocks for Mixing Controlled Compression Ignition Combustion. SAE Tech. Pap., vol. 2019- April, 2019, p. 1–22. doi: 10.4271/2019-01-0570.

[47] Abel RC, Luecke J, Ratcliff MA, Zigler BT. Comparing Cetane Number Measurement Methods. ASME 2020 Intern. Combust. Engine Div. Fall Tech. Conf., American Society of Mechanical Engineers; 2020, p. 1–10. doi: 10.1115/ICEF2020-3017.

[48] Ran Z, Longtin J, Assanis D. Investigating anode off-gas under spark-ignition combustion for SOFC-ICE hybrid systems. 146808742110169 Int J Engine Res 2021. https://doi.org/10.1177/14680874211016987.

[49] Li Z, Liu G, Cui X, Sun X, Li S, Qian Y, et al. Effects of the variation in diesel fuel components on the particulate matter and unregulated gaseous emissions from a common rail diesel engine. Fuel 2018;232:279–89. https://doi.org/10.1016/j.fuel.2018.05.170.

[50] Reşitoğlu İA, Altinişik K, Keskin A. The pollutant emissions from diesel-engine vehicles and exhaust aftertreatment systems. Clean Technol Environ Policy 2015; 17(1):15–27. https://doi.org/10.1007/s10098-014-0793-9.